Bending a photonic wire into a ring

Henrik Gotfredsen,[†1] Jie-Ren Deng,[†1] Jeff M. Van Raden,[1] Marcello Righetto,[2] Janko Hergenhahn,[1] Michael Clarke,[3] Abigail Bellamy-Carter,[3] Jack Hart,[3] James O'Shea,[3] Timothy D. W. Claridge,[1] Fernanda Duarte,[1] Alex Saywell,*[3] Laura M. Herz,*[2] and Harry L. Anderson*[1]

(† These authors contributed equally)

1. Department of Chemistry, University of Oxford, Chemistry Research Laboratory, Oxford OX1 3TA, UK

2. Department of Physics, University of Oxford, Clarendon Laboratory, Parks Road, Oxford OX1 3PU, UK

3. School of Physics & Astronomy, University of Nottingham, Nottingham, NG7 2RD, UK

*Correspondence to: harry.anderson@chem.ox.ac.uk, laura.herz@physics.ox.ac.uk or alex.saywell@nottingham.ac.uk

Natural light-harvesting systems absorb sunlight and transfer its energy to the reaction centre, where it is used for photosynthesis. Synthetic chromophore arrays provide useful models for understanding energy migration in these systems. Research has focussed on mimicking rings of chlorophyll molecules found in purple bacteria, known as 'light-harvesting system 2'. Linear *meso-meso* linked porphyrin chains mediate rapid energy migration, but until now it has not been possible to bend them into rings. Here we show that oligo-pyridyl templates can be used to bend these rod-like photonic wires to create covalent nanorings that consist of 24 porphyrin units and a single butadiyne link. Their elliptical conformations have been probed by scanning tunnelling microscopy. This system exhibits two excited state energy transfer processes: one from a bound template to the peripheral porphyrins and one, in the template-free ring, from the exciton-coupled porphyrin array to the π-conjugated butadiyne-linked porphyrin dimer segment.

Green plants, and other photosynthetic organisms, capture sunlight using antenna complexes that consist of large arrays of chlorophyll molecules. Electronic excitation is funnelled through the antenna complex into a reaction centre, where it is converted into chemical energy[1,2]. There are typically 100–800 light-absorbing chlorophyll units per reaction centre[3], and each absorption event results in a long cascade of electronic excitation energy transfer (EET) steps. Light harvesting systems have evolved so that this EET process is

extremely rapid, and it occurs efficiently without significant competition from other decay channels, such as fluorescence, intersystem crossing and non-radiative internal conversion. Different organisms use a wide variety of light-harvesting chlorophyll antenna complexes. Two of the most highly studied examples are light-harvesting systems 1 and 2 (LH1 and LH2) from purple bacteria[1]. LH2 consists of two concentric rings of bacteriochlorophyll units (both with diameters of ~6 nm)[4]: the B800 ring of 9 chlorophylls and the B850 ring of 18 chlorophylls. The B850 ring is remarkable because its 18 bacteriochlorophyll units are closely spaced and strongly coupled, resulting in ultra-fast intra-ring EET (<200 fs)[2]. Many rings of porphyrin units have been synthesised and investigated as models for LH2[5-12], but in most cases the EET in these models is much slower than in the natural B850 ring. The only synthetic cyclic porphyrin arrays that mimic intra-ring EET on the same time scale (<200 fs) and length scale (~6 nm diameter) as the B850 ring are the butadiyne-linked porphyrin nanorings developed in our laboratories[8,9]. However, these rings achieve strong porphyrin-porphyrin coupling through π-conjugation (i.e. direct orbital overlap), which makes them fundamentally different from the exciton-coupled rings of chlorophyll units in LH2. In this paper, we explore the synthesis and photophysical properties of rings consisting of closely spaced exciton-coupled porphyrin units, with diameters of about 6 nm, which exhibit ultrafast EET.

Kim, Osuka and coworkers have shown that directly *meso-meso* linked linear porphyrin arrays (***l*-P*N***, Figure 1) behave as 'photonic wires' and exhibit ultrafast EET due to strong exciton coupling between neighbouring porphyrin units, with radiative coherence lengths of about 4–6 porphyrin units[13–15]. The corresponding cyclic 5,15-linked porphyrin nanorings (***c*-P*N***, Figure 1) would be fascinating models for LH2, but it would be difficult to study EET in these highly symmetric rings because there would be no directional energy flow[16]. It would be easier to probe EET in structures such as ***c*-P*N*b**, with a single butadiyne link, because excitation would then migrate to the site of the butadiyne, because a π-conjugated butadiyne-linked porphyrin dimer has a lower S_1 excited state than a *meso-meso* linked porphyrin oligomer. The single butadiyne link in ***c*-P*N*b** also makes it easier to synthesise. Here we report the template-directed synthesis of a 24-porphyrin nanoring of this type with a single butadiyne link. Oligomers of the type ***l*-P*N*** are often described as "rodlike"[13], which raises the question of whether we can bend a straight rod into a ring. Here we show that molecular templates can be used to enforce a circular geometry to create this strained nanoring.

Results and Discussion

Computational modelling and design of the template. We started this project by calculating the strain in ***c*-P*N*** and ***c*-P*N*b**, as a function *N*, by considering gas-phase homodesmotic reactions, using both molecular mechanics calculations and density functional theory (DFT) (see Supplementary Information for details). As expected, the level of strain is high in the smaller macrocycles (e.g. ***c*-P12**: 155.8 kJ mol^{-1} and ***c*-P12b**: 143.5 kJ mol^{-1}), but declines as the rings become larger. Thus the strain energies of ***c*-P24** (78.7 kJ mol^{-1}) or ***c*-P24b** (75.7 kJ mol^{-1}) are less than in the alkyne-linked porphyrin nanorings that we have reported previously (100–130 kJ mol^{-1})[17], implying that they are reasonable targets for template-directed synthesis.

One challenge in designing a template to bind a linear oligo-porphyrin, such as ***l*-P24e**, to direct the formation of ***c*-P24b**, is that *meso-meso* singly-linked oligomers have twisted conformations[18,19]. The dihedral angle between neighbouring zinc porphyrins is typically 70–90°, so that the axial vectors of the porphyrin units in ***c*-P24b** do not point towards the centre of the nanoring. Inspired by the work of Osuka and coworkers[18] on the binding of α,ω-diaminoalkanes to dimers such as ***l*-P2**, we designed a binding unit **L**, which has two 4-pyridyl binding sites connected to a benzene core via flexible *meta*-linked -O(CH$_2$)$_3$- chains. Computational studies indicated that this ligand would coordinate the two zinc centres of the twisted porphyrin dimer ***l*-P2** and this was confirmed by UV-vis binding studies, which gave a binding constant 7.8×10^5 M^{-1} (in $CDCl_3$ at 298 K), compared with 1.2×10^4 M^{-1} for the **P1** monomer binding 4-ethyl pyridine, under identical conditions. Although the effective molarity of this system is quite low (*EM* = 2.7 mM), it is high enough for the ***l*-P2·L** complex to be 94% closed (i.e. coordinated at both sites)[20].

It would be difficult to design a single template capable of binding all 24 zinc sites in ***l*-P24e**, to bend it into a circular conformation. Instead, we designed the **T12** template, which has six **L** binding units linked to a benzene core, and is shaped so that a cofacial stack of two molecules of **T12** can bind inside the cavity of ***c*-P24b** (Figure 3)[21]. Molecular dynamics simulations of ***l*-P24e·(T12)$_2$** predicted that all 24 of the pyridyl binding sites of the templates remain coordinated to zinc atoms in the 1:2 complex. General AMBER force field[22] parameters were employed together with novel hybrid bonded/non-bonded parameters for the zinc ions that were adjusted to reproduce the coordination geometry and energy of pyridine zinc interactions. The ***l*-P24e·(T12)$_2$** complex is predicted to exist as two

isomers with similar energies (binding modes A and B, Figure 4). The angle θ and distance d between the terminal alkynes fluctuates across a distribution of values in these complexes (Figure 4b,c), including those in a range suitable for Glaser coupling[23]. There is no strong correlation between the two parameters, θ and d, because the alkynes tend to move apart by displacement away from the mean plane of the complex, rather than unwrapping from the templates.

Synthesis and chemical characterisation. Palladium-catalysed oxidative coupling of ***l*-P24e** in the presence of **T12**, followed by displacement of the template with pyridine, gave nanoring ***c*-P24b** in 26% yield (Figure 3). This compound was initially identified from its retention time by gel-permeation chromatography (GPC) and by observation of its molecular ion in mass spectrometry (found *m/z* 24,927.5; calc. $C_{1540}H_{1968}N_{96}O_{96}Zn_{24}$: 24,930.0). The GPC retention time of ***c*-P24b** is 4.6% longer than that of ***l*-P24e**, as expected for the smaller hydrodynamic radius of the cyclic compound[24]. The same effect is seen by diffusion-ordered NMR spectroscopy (DOSY): ***c*-P24b** and ***l*-P24** have diffusion coefficients of 1.37×10^{-10} $m^2\ s^{-1}$ and 9.40×10^{-11} $m^2\ s^{-1}$, respectively, in $CDCl_3$ at 298 K. The ^1H NMR spectrum of ***c*-P24b** resembles that of ***l*-P24e**, except without the terminal alkyne peak at δ_H 4.28 ppm. The many similar unresolved porphyrin ^1H NMR environments of the cyclic compound also show a wider chemical shift dispersion than for the linear chain.

The interaction of the nanoring ***c*-P24b** with template **T12** was studied by UV-vis and fluorescence titrations (in $CDCl_3$ at 298 K). The formation titration confirms that ***c*-P24b** binds strongly with two equivalents of **T12** to give a 1:2 complex ***c*-P24b·(T12)$_2$** (Supplementary Figures 20, 21). The formation constant (K_f) is too high to measure directly from the formation titration, and denaturation titrations, in which a competing ligand (quinuclidine) is added to displace the template, were used to determine the stability of the complex[25]. Displacement of **T12** from ***c*-P24b·(T12)$_2$** with increasing quinuclidine concentration can be monitored by the turn-on response of fluorescence at 472 nm, because the free **T12** template is highly florescent, whereas its fluorescence is quenched in the complex (due to energy transfer to the porphyrin nanoring, as shown below). Analysis of the binding isotherms shows that the 1:2 complex ***c*-P24b·(T12)$_2$** is extremely stable with $\log(K_f) = 81.5 \pm 0.7$, $\Delta G = 465$ kJ mol^{-1}, which illustrates that there is ample binding energy to overcome the strain energy required to form the nanoring. The effective molarity for formation of ***c*-P24b·(T12)$_2$** (EM = 0.2 M) is two orders of magnitude greater than for the

reference system **L·*l*-P2** (*EM* = 2.7 mM), reflecting the shape-complementarity between the template and the nanoring.

We also attempted to synthesise a smaller nanoring ***c*-P12b** using two smaller versions of **T12**, but no cyclic products were formed from ***l*-P12e** in either case. This can probably be attributed to the high strain in ***c*-P12b** (see Supplementary Information, Section 4 and Figure 5).

Scanning probe microscopy. The ***c*-P24b** nanoring was transferred from solution in toluene/methanol onto a Au(111) substrate, held under vacuum conditions, by electrospray deposition using a previously reported procedure[26]. Images of the molecules were recorded by scanning tunnelling microscopy (STM), as illustrated in Figure 5a,b (and Supplementary Figures 12–15). The variation in contrast around the nanorings is attributed to the non-planar orientation of the porphyrin sub-units, with the brighter features assigned to porphyrins tilted upwards from the surface plane. The measured long and short axes of the rings indicate some structural flexibility. Average values of the long axis (a = 6.9 nm, SD 0.9 nm) and short axis (b = 4.3 nm, SD 0.7 nm) correspond to an ellipticity or flattening factor of $f = 1 - b/a = 0.4$ (SD = 0.2) on the gold surface, which is significantly greater than for the optimised geometry from DFT (a = 6.8 nm; b = 6.4 nm; f = 0.07; Figure 5c). The distribution of conformations observed by STM is compared with that from molecular dynamics calculations (at 300 K with explicit $CHCl_3$ solvent; a = 6.9 nm, SD 0.3 nm; b = 5.8 nm, SD 0.3 nm; f = 0.16, SD 0.07) in Figure 5d. The mean circumference from the molecular dynamics calculations (c = 20.0 nm) is slightly larger than the apparent average circumference from the STM images (18.2 nm, for the average of 38 images), but this probably reflects the fact that the molecules on the surface are not exactly elliptical. Interactions with substrate features, such as step-edges and the herringbone reconstruction of Au(111), may favour alternative conformations to those predicted by solution-phase calculations. The nanorings display significant mobility under these measurement conditions, with several lateral translation events observed (diffusion occurs at a faster rate than the acquisition time of an STM image and translation events are highlighted with arrows in Figure 5a). This mobility indicates a decreased adsorption energy compared to the butadiyne-linked variant, which can be attributed to the nonplanarity of ***c*-P24b**.

Photophysics and excited-state energy transfer. The UV-visible absorption and fluorescence spectra of ***c*-P24b** and ***l*-P24** are compared with those of a porphyrin tetramer

with a central butadiyne link, ***l*-P4b**, in Figure 6a,b. The absorption spectra of ***c*-P24b** and ***l*-P24** feature intense bands at 419, 515 and 594 nm which are assigned to the B_y, B_x and Q transition, respectively[13]. The absorption spectra of ***c*-P24b** and ***l*-P4b** also feature a weaker band at 650–700 nm, which is not present for ***l*-P24** and which is attributed to the π-conjugated butadiyne-linked porphyrin dimer unit (Figure 6a, insert). The fluorescence spectra of ***c*-P24b** and ***l*-P4b** are very similar with peaks at 729 and 723 nm respectively (Figure 6b), and both compounds emit at a longer wavelength than ***l*-P24** (λ_{max} 651 nm), which indicates that EET to the butadiyne-linked porphyrin dimer unit occurs efficiently in ***c*-P24b**. Comparison of the emission intensities at 651 and 729 nm in the steady-state fluorescence spectra of ***l*-P24**, ***l*-P4b** and ***c*-P24b** (Figure 6b) implies that the EET efficiency is >93%.

The EET process in ***c*-P24b** was investigated by monitoring the evolution of its fluorescence on a ps-timescale through fluorescence up-conversion spectroscopy (time resolution: ~350 fs). The fluorescence from ***c*-P24b** displays a rapid decay at 650 nm and a concomitant rise at 720 nm (Figures 6c, and Supplementary Figures 35 and 36). A stretched exponential decay, equation (1), provides an excellent description of the 650 nm emission kinetics for the ring (see Supplementary Information, Section 9).[27]

$$I(t) = I_0 \exp\left[-(t/\tau_0)^{\beta}\right] \quad (1)$$

where $I(t)$ is the fluorescence intensity, t is time, τ_0 is the time constant and β is the stretching exponent. The extracted parameters are $\tau_0 = 8.5 \pm 0.6$ ps and $\beta = 0.54 \pm 0.04$. The stretching exponent is significantly below unity (monoexponential decay), indicating that a range of excitation transfer times is present, as expected for random placement of excitation across the different porphyrins units comprising the ring. The characteristic transfer time τ_0 represents an average time taken for an excitation to migrate from porphyrin donors to the butadiyne-linked porphyrin dimer acceptor unit. The matching rise dynamics observed in the emission at 720 nm confirms that these coupled dynamics are associated with energy transfer. Modelling of the transient fluorescence at 650 and 720 nm (Figure 6c, and Supplementary Figure 36) with an exciton generation function (Supplementary Information, equation 14) indicates that approximately 40% of the excitation arrives at the butadiyne-linked porphyrin unit within the time-resolution. We estimate from the absorption spectra (Figure 6a) that 9% of the absorption at 410 nm is direct excitation of the butadiyne-linked acceptor site, which implies that about 30% of the EET occurs within the time resolution

(350 fs). Further evidence of EET is provided by the pronounced redshift of the peak emission wavelength in ***c*-P24b**, during 0–50 ps after excitation (Figure 6d,e). Again, it is clear that part of the EET occurs within the time resolution, because the emission maximum of ***c*-P24b** is redshifted with respect to that of ***l*-P24** even at the earliest times we can measure (Figure 6e). On a longer timescale (~500 ps), the emission spectrum of ***c*-P24b** exhibits a slower redshift due to planarisation of the excited state of the butadiyne-linked porphyrin dimer unit[28,29]; this slow process is also observed in ***l*-P4b**. In contrast, ***l*-P24** displays only weak shifts due to EET among segments of the chain with different porphyrin-porphyrin dihedral angles.[13] It is interesting that the average rate of EET in ***c*-P24b** is significantly faster than in a similar linear 24-porphyrin chain terminated with an ethynyl-porphyrin energy acceptor (time constant 110 ps)[30,31].

Energy transfer is also observed from the central template units in ***c*-P24b·(T12)$_2$** to the surrounding zinc porphyrins. The **T12** template is highly fluorescent (λ_{em}: 472 nm; ϕ_f = 0.26, in toluene at 298 K) and its fluorescence is quenched (by a factor of 99.6%) in the ***c*-P24b·(T12)$_2$** complex, as mentioned above and shown in Figure 6f. The excitation spectrum of ***c*-P24b·(T12)$_2$**, based on emission at 760 nm, has a peak at 319 nm corresponding to the absorption spectrum of the template (Supplementary Figure 30), which demonstrates that there is energy transfer from the **T12** unit to the porphyrin manifold. Analysis of transient fluorescence decays (inset of Figure 6f) reveals an average energy transfer time of 0.15 ns. EET from *meso*-*meso*-linked porphyrins to the butadiyne-linked porphyrin dimer unit in ***c*-P24b·(T12)$_2$** is much less efficient than in ***c*-P24b**, as indicated by the broad fluorescence spectrum of ***c*-P24b·(T12)$_2$**, which extends from around 650 nm to 750 nm (Supplementary Figure 30). Molecular dynamics simulations provide an explanation for the reduced efficiency of EET in ***c*-P24b·(T12)$_2$**: the **T12** template tends to hold the butadiyne-linked porphyrins in a twisted conformation, with the two porphyrins orthogonal. This conformation is not π-conjugated and it has a higher energy S_1 excited state[28], so that the butadiyne-linked porphyrins cease to constitute an effective energy acceptor when the nanoring is bound to two **T12** units.

Conclusion

This work demonstrates that oligo-pyridine templates can be used to direct the synthesis of large zinc porphyrin nanorings, even from linear oligomers that are twisted and rod-like. It also illustrates the power of molecular dynamics simulations to guide the design of

templates. STM images confirm that the nanorings adopt elliptical conformations, similar to those predicted computationally. Excited state energy transfer from the 22 *meso-meso* linked porphyrin units to the butadiyne-linked segment of ***c*-P24b** occurs over a range of time scales, as expected from the distribution of donor-acceptor distances. About 30% of the energy is transferred within the time resolution of our measurements (350 fs), while the EET process has an average time constant of 8.5 ps. The ***c*-P24b** macrocycle has a similar size to the B850 ring of LH2, and a similar distance between neighbouring porphyrin units. However, in ***c*-P24b** neighbouring porphyrins are almost orthogonal, whereas in B850 they are essentially parallel. This difference in geometry probably accounts for the slower EET in ***c*-P24b**.

Acknowledgments. We thank the ERC (grant 885606, ARO-MAT) for funding. H.G. thanks the Independent Research Fund Denmark for an International Postdoctoral Fellowship. A.S. thanks the Royal Society for support via a University Research Fellowship. Computational services were provided by the Advanced Research Computing Service at the University of Oxford. M.R. and L.M.H. acknowledge funding by the Engineering and Physical Sciences Research Council UK. L.M.H. acknowledges support through a Hans Fischer Senior Fellowship from the Technical University of Munich's Institute for Advanced Study, funded by the German Excellence Initiative.

Author contributions

H.G., J.-R.D. and J.M.V.R. synthesised and characterised the compounds. J.H. and F.D. carried out the computational modelling, after preliminary modelling by H.G., J.-R.D. and J.M.V.R.; T.D.W.C. assisted with NMR experiments; A.B.-C., M.C. and A.S. performed the scanning probe microscopy. J.H. and J.O. prepared samples via electrospray deposition. M.R. and L.M.H. investigated the time-resolved photophysics. H.L.A. and H.G. wrote the paper; all authors discussed the results and edited the manuscript.

Competing interests

The authors declare no competing interests.

Figure Legends/Captions (for main text figures) and graphics

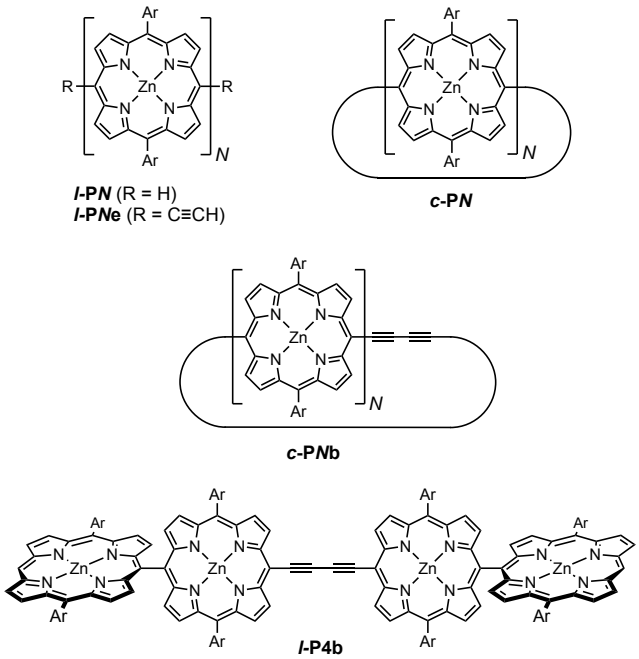

Fig. 1 | Structures of porphyrin oligomers, ***l*-P*N***, ***l*-P*N*e**, ***c*-P*N*** and ***c*-P*N*b** (where *N* is the number of porphyrin units; ***l*-**, ***c*-**, **e** and **b** indicate linear, cyclic, ethynyl and butadiyne, respectively), and the reference compound ***l*-P4b**. Ar is the 3,5-bis(octyloxy)phenyl solubilising group.

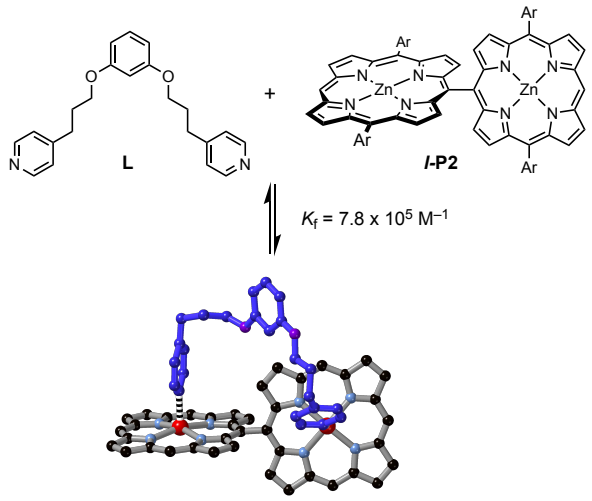

Fig. 2 | Chelation of the binding unit L to *l*-P2. The binding constant (7.8×10^5 M^{-1}) was measured by UV-vis titration in $CDCl_3$ at 298 K and compares with a value of 1.2×10^4 M^{-1} for the corresponding **P1** monomer binding 4-ethyl pyridine. The optimised geometry of ***l*-P2·L** was calculated using DFT (PBE0+GD3BJ/Def2SVP). Ar = 3,5-bis(octyloxy)phenyl.

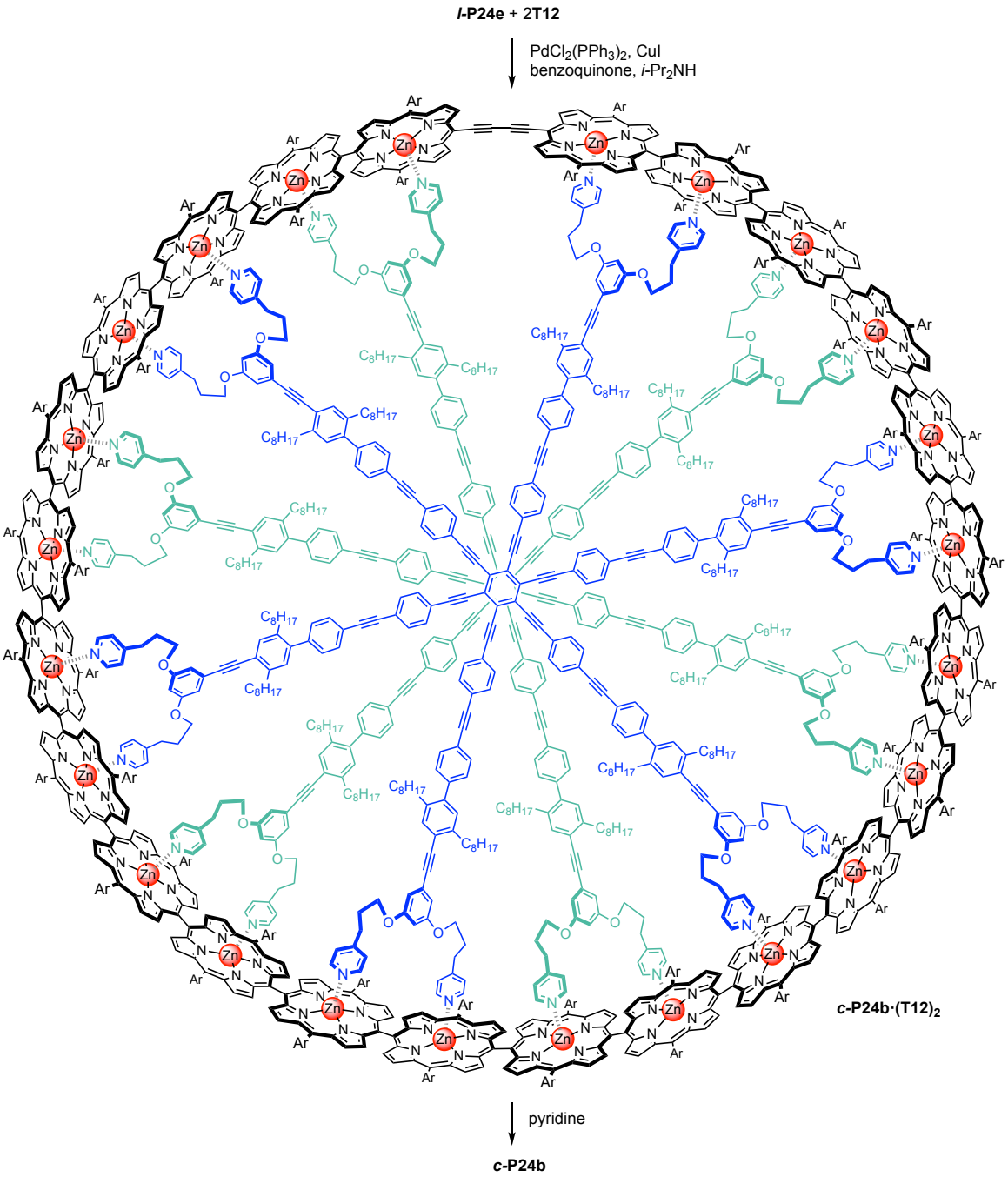

Fig. 3 | Reaction scheme showing the synthesis of *c*-P24b via the template complex *c*-P24b·(T12)$_2$. The solubilising side chains on all the porphyrins are Ar = 3,5-bis(octyloxy)phenyl.

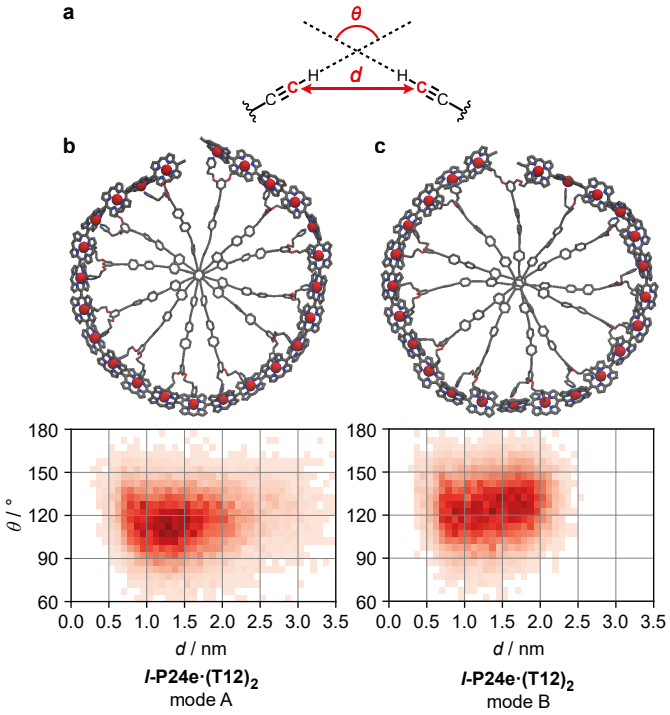

Fig. 4 | Molecular dynamics simulations of *l*-P24e·(T12)$_2$. a, Definition of parameters *d* and *θ*. **b** and **c**, Geometry distributions for the two binding modes A and B with structures representative of the highest probabilities of *d* and *θ*.

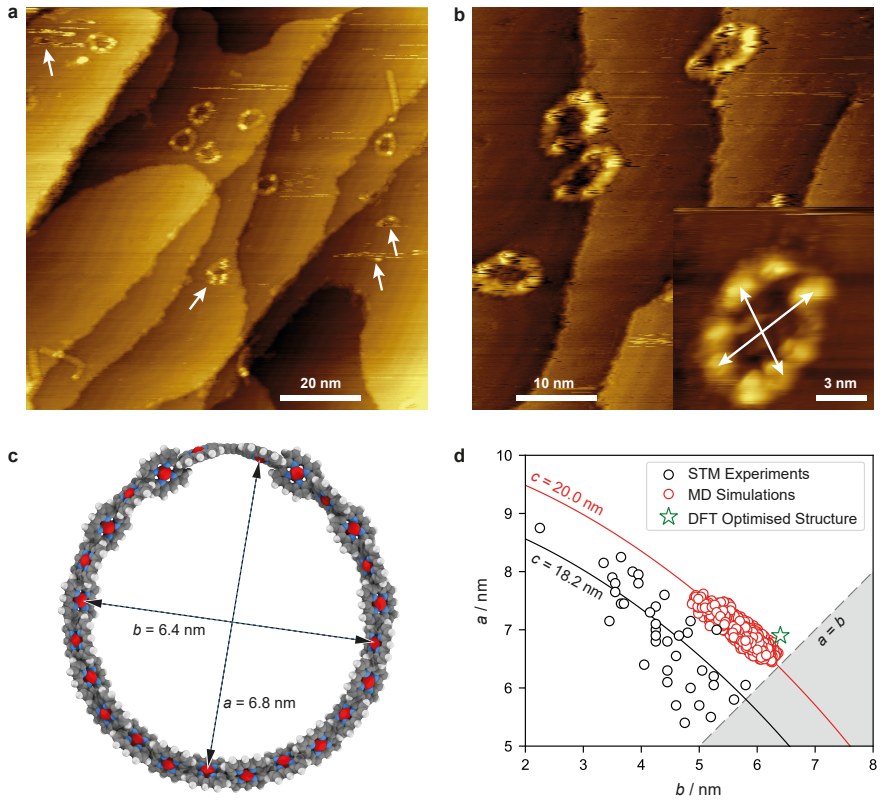

Fig. 5 | STM characterisation of *c*-P24b on Au(111). a-b, STM-images of the ***c*-P24b** nanoring deposited on a Au(111) surface under UHV (–1.8 V sample-bias, 20 pA set-point current, T = 293 K, image sizes; 100 × 100 nm, 50 × 50 nm, and 12 × 12 nm). In panel (a), arrows indicate ***c*-P24b** nanorings which are mobile on the timescale of image acquisition. In panel (b), arrows show an example of the measured dimensions. **c**, Optimised geometry of ***c*-P24b** (PBE0+GD3BJ/Def2SVP). Aryl and octyl solubilising groups were replaced by hydrogen to simplify the calculations. **d**, plot of long (a) vs. short (b) axes values for 38 rings observed by STM (black circles) and points from the molecular dynamics simulation (red circles). The black and red curves are the corresponding best fit lines for ellipses of fixed circumference (c = 18.2 nm and 20.0 nm, respectively, calculated using Ramanujan's approximation). The dashed line indicates circular geometries, $a = b$.

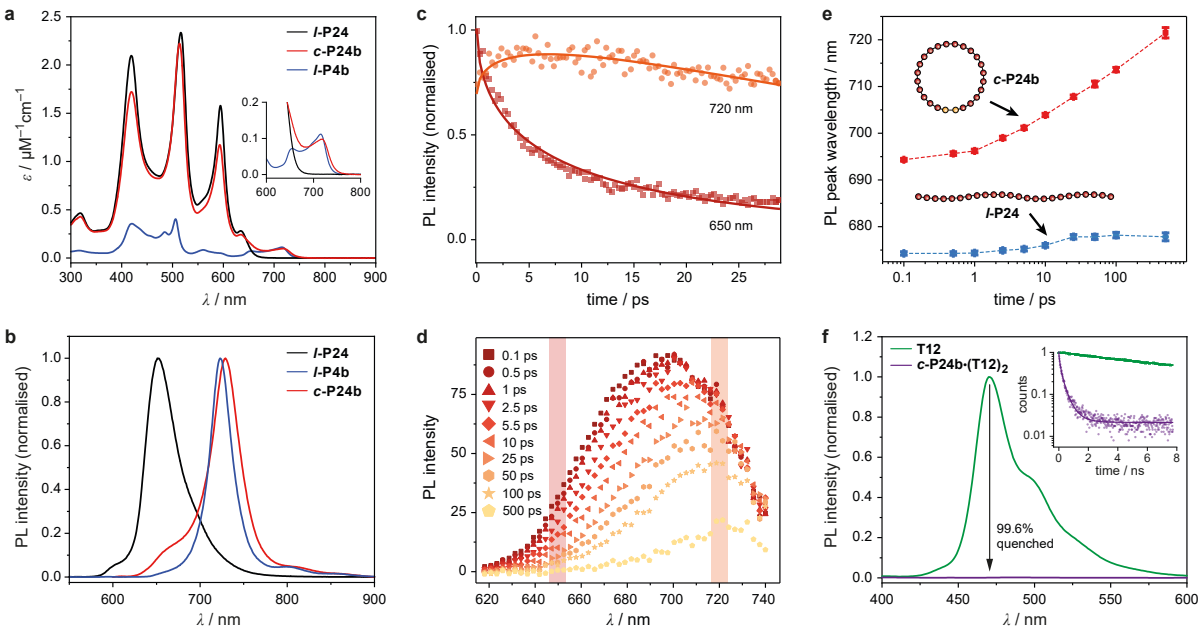

Fig. 6 | Absorption and fluorescence spectra. a, UV-vis absorption spectra. **b**, Steady-state fluorescence spectra. (Excitation wavelength: 515 nm for ***c*-P24b** and ***l*-P24**; 505 nm for ***l*-P4b**.) **c**, Transient fluorescence of ***c*-P24b**, detected at 650 nm (red squares) and 720 nm (orange circles) under 410 nm wavelength excitation at 2.5 μJ cm^{-2}. Solid lines represent fits to the model described in Supplementary Information, Section 9. **d**, Time-resolved fluorescence spectra for ***c*-P24b** following 410-nm wavelength pulsed excitation at a fluence of 2.5 μJ cm^{-2}. Different symbols represent spectra taken at different times after the excitation, in the range 100 fs (dark red square) – 500 ps (yellow pentagon). **e**, Comparison between the time evolution of the peak wavelength of the photoluminescence spectra for ***c*-P24b** (red squares), and ***l*-P24** (blue circles). Data points are extracted through Gaussian fitting of the time-resolved photoluminescence spectra measured under the same excitation as a function of time after excitation. Dashed lines are guides for the eye. **f**, Emission spectra of **T12** (1.6×10^{-7} M) and ***c*-P24b·(T12)$_2$** (0.8×10^{-8} M), i.e. at identical template concentration, with excitation at 318 nm. The **T12** quenching efficiency in the complex is 99.6%. The insert shows the transient fluorescence decay from both solutions (excitation wavelength: 380 nm, power 6 mW). The free template exhibits a mono-exponential decay $\tau = 8 \pm 1$ ns. The template emission can be fitted with stretched exponential decay ($\tau_0 = 0.15 \pm 0.04$ ns; □ = 0.7). All spectra were recorded in toluene containing 1% pyridine at 298 K, except for ***c*-P24b·(T12)$_2$** which was dissolved in toluene without pyridine.

References

1. Cogdell, R. J., Gall, A. & Köhler, J. The architecture and function of the light-harvesting apparatus of purple bacteria: from single molecules to *in vivo* membranes. *Q. Rev. Biophys.* **39**, 227–324 (2006).

2. Mirkovic, T., Ostroumov, E. E., Anna, J. M., van Grondelle, R., Govindjee & Scholes, G. D. Light absorption and energy transfer in the antenna complexes of photosynthetic organisms. *Chem. Rev.* **117**, 249−293 (2017).

3. Mauzerall, D. & Greenbaum, N. L. The absolute size of a photosynthetic unit. *Biochim. Biophys. Acta* **974**, 119−140 (1989).

4. McDermott, G., Prince, S. M., Freer, A. A., Hawthornthwaite-Lawless, A. M., Papiz, M. Z., Cogdell, R. J. & Isaacs, N. W. Crystal structure of an integral membrane light-harvesting complex from photosynthetic bacteria. *Nature* **374**, 517–521 (1995).

5. Cho, H. S., Rhee, H., Song, J. K., Min, C.-K., Takase, M., Aratani, N., Cho, S., Osuka, A., Joo, T. & Kim, D. Excitation energy transport processes of porphyrin monomer, dimer, cyclic trimer, and hexamer probed by ultrafast fluorescence anisotropy decay. *J. Am. Chem. Soc.* **125**, 5849–5860 (2003).

6. Choi, M.-S., Yamazaki, T., Yamazaki, I. & Aida, T. Bioinspired molecular design of light-harvesting multiporphyrin arrays. *Angew. Chem. Int. Ed.* **43**, 150–158 (2004).

7. Aratani, N., Kim, D. & Osuka, A. Discrete cyclic porphyrin arrays as artificial light-harvesting antenna. *Acc. Chem. Res.* **42**, 1922–1934 (2009).

8. Parkinson, P., Kondratuk, D. V., Menelaou, C., Gong, J. Q., Anderson, H. L. & Herz, L. M. Chromophores in molecular nanorings: When is a ring a ring? *J. Phys. Chem. Lett.* **5**, 4356−4361 (2014).

9. Yong, C.-K., Parkinson, P., Kondratuk, D. V., Chen, W.-H., Stannard, A., Summerfield, A., Sprafke, J. K., O'Sullivan, M. C., Beton, P. H., Anderson, H. L. & Herz, L. M. Ultrafast delocalization of excitation in synthetic light-harvesting nanorings. *Chem. Sci.* **6**, 181–189 (2015).

10. Otsuki, J. Supramolecular approach towards light-harvesting materials based on porphyrins and chlorophylls. *J. Mater. Chem. A* **6**, 6710–6753 (2018).

11. Yang, J., Yoon, M.-C., Yoo, H., Kim, P. & Kim, D. Excitation energy transfer in multiporphyrin arrays with cyclic architectures: towards artificial light-harvesting antenna complexes. *Chem. Soc. Rev.* **41**, 4808–4826 (2012).

12. Aratani, N. & Osuka, A. Exploration of giant functional porphyrin arrays. *Bull. Chem. Soc. Jpn.* **88**, 1–27 (2015).

13. Kim, Y. H., Jeong, D. H., Kim, D., Jeoung, S. C., Cho, H. S., Kim, S. K., Aratani, N. & Osuka, A. Photophysical properties of long rodlike *meso-meso*-linked zinc(II) porphyrins investigated by time-resolved laser spectroscopic methods. *J. Am. Chem. Soc.* **123**, 76–86 (2001).

14. Ha, J.-H., Cho, H. S., Song, J. K., Kim, D., Aratani, N. & Osuka, A. Excitonic coupling strength and coherence length in the singlet and triplet excited states of *meso–meso* directly linked Zn(II)porphyrin arrays. *ChemPhysChem* **5**, 57– 67 (2004).

15. Yang, J., Yoo, H., Aratani, N., Osuka, A. & Kim, D. Determination of the superradiance coherence length of directly linked linear porphyrin arrays at the single-molecule level. *Angew. Chem. Int. Ed.* **48**, 4323–4327 (2009).

16. Van Patten, P. G., Shreve, A. P., Lindsey, J. S., Donohoe, R. J. Energy-transfer modeling for the rational design of multiporphyrin light-harvesting arrays. *J. Phys. Chem. B* **102**, 4209–4216 (1998).

17. Haver, R., Tejerina, L., Jiang, H.-W., Rickhaus, M., Jirasek, M., Grübner, I., Eggimann, H. J., Herz, L. M. & Anderson, H. L. Tuning the circumference of six-porphyrin nanorings. *J. Am. Chem. Soc.* **141**, 7965−7971 (2019).

18. Shinmori, H., Ahn, T. K., Cho, H. S., Kim, D., Yoshida, N. & Osuka, A. Dihedral-angle modulation of *meso–meso*-linked Zn^{II} diporphyrin through diamine coordination and its application to reversible switching of excitation energy transfer. *Angew. Chem. Int. Ed.* **42**, 2754–2758 (2003).

19. Yoshida, N., Ishizuka, T., Osuka, A., Jeong, D. H., Cho, H. S., Kim, D., Matsuzaki, Y., Nogami, A. & Tanaka, K. Fine tuning of photophysical properties of *meso–meso*-linked Zn^{II}–diporphyrins by dihedral angle control. *Chem. Eur. J.* **9**, 58–75 (2003).

20. Hunter, C. A. & Anderson, H. L. What is cooperativity? *Angew. Chem. Int. Ed.* **48**, 7488–7499 (2009).

21. Bols, P. S.; Rickhaus, M., Tejerina, L.; Gotfredsen, H., Eriksen, K., Jirasek, M. & Anderson, H. L. Allosteric cooperativity and template-directed synthesis with stacked ligands in porphyrin nanorings. *J. Am. Chem. Soc*. **142**, 13219−13226 (2020).

22. Wang, J. M., Wolf, R. M., Caldwell, J. W., Kollman, P. A. & Case, D. A. Development and testing of a general amber force field. *J. Comput. Chem*. **25**, 1157–1174, (2004).

23. Fomina, L., Vazquez, B., Tkatchouk, E. & Fomine, S. The Glaser reaction mechanism. A DFT study. *Tetrahedron* **58**, 6741–6747 (2002).

24. Kondratuk, D. V., Perdigão, L. M. A., Esmail, A. M. S., O'Shea, J. N., Beton, P. H. & Anderson, H. L. Supramolecular nesting of cyclic polymers. *Nat. Chem.* **7**, 317–322 (2015).

25. Hogben, H. J., Sprafke, J. K., Hoffmann, M., Pawlicki, M., & Anderson, H. L. Stepwise effective molarities in porphyrin oligomer complexes: preorganization results in exceptionally strong chelate cooperativity. *J. Am. Chem. Soc.* **133**, 20962–20969 (2011).

26. Judd, C. J.; Nizovtsev, A. S.; Plougmann, R.; Kondratuk, D. V.; Anderson, H. L.; Besley E. & Saywell, A. Molecular quantum rings formed from a π-conjugated macrocycle. *Phys. Rev. Lett.* **125**, 206803 (2020).

27. Berberan-Santos, M. N., Bodunov, E. N. & Valeur, B. Mathematical functions for the analysis of luminescence decays with underlying distributions 1. Kohlrausch decay function (stretched exponential). *Chem. Phys.* **315**, 171–182 (2005).

28. Winters, M. U., Kärnbratt, J., Eng, M., Wilson, C. J., Anderson, H. L. & Albinsson, B. Photophysics of a butadiyne-linked porphyrin dimer: Influence of conformational flexibility in the ground and first singlet excited state. *J. Phys. Chem. C* **111**, 7192–7199 (2007).

29. Chang, M.-H., Hoffmann, M., Anderson, H. L. & Herz, L. M. Dynamics of excited-state conformational relaxation and electronic delocalization in conjugated porphyrin oligomers. *J. Am. Chem. Soc.* **130**, 10171–10178 (2008).

30. Aratani, N., Cho, H. S., Ahn, T. K., Cho, S., Kim, D., Sumi, H. & Osuka, A. Efficient excitation energy transfer in long *meso-meso* linked Zn(II) porphyrin arrays bearing a 5,15-bisphenylethynylated Zn(II) porphyrin acceptor. *J. Am. Chem. Soc.* **125**, 9668–9681 (2003).

31. Ahn, T. K., Yoon, Z. S., Hwang, I.-W., Lim, J. K., Rhee, H., Joo, T., Sim, E., Kim, S. K., Aratani, N., Osuka, A. & Kim, D. Effect of conformational heterogeneity on excitation energy transfer efficiency in directly *meso-meso* linked Zn(II) porphyrin arrays. *J. Phys. Chem. B* **109**, 11223–11230 (2005).

Additional information

Supplementary information is available for this paper at https://doi.org/10.?????

Methods

Synthesis of *c*-P24b. A solution of **T12** template (5.3 mg, 1.0 μmol, 2.0 equiv) in $CHCl_3$ (220 mL) was added to a solution of linear 24-mer ***l*-P24e** (12.5 mg, 0.50 μmol) in $CHCl_3$ (250 mL). A catalyst mixture was prepared by dissolving CuI (54 mg, 284 μmol), $Pd(PPh_3)_2Cl_2$ (39 mg, 56 μmol), and 1,4-benzoquinone (121 mg, 1120 μmol) in DIPA (1.2 mL) and $CHCl_3$ (48 mL) using sonication. The catalyst mixture was added to the reaction flask and stirred under air for 18 h, while monitoring the reaction by analytical GPC. A solution of pyridine (0.5 mL) in THF (50 mL) was added to the reaction mixture and it was concentrated under reduced pressure to a volume of ca. 10 mL, then passed through a short size-exclusion column (Bio-Beads S-X1, THF + 1% pyridine) to remove unreacted 1,4-benzoquinone and copper salts. Purification by recycling GPC (loading in THF + 20% pyridine; eluting in THF + 1% pyridine), followed by further size-exclusion chromatography (Bio-Beads S-X1, $CHCl_3$) gave ***c*-P24b** as a black solid (3.22 mg, 26%). See Supplementary Information for characterisation data and related compounds.

Molecular Dynamics. All simulations were performed in an isothermal-isobaric (NPT) ensemble at 300 K and 1 bar with a time step of 2 fs using GROMACS (v. 2019.2).[32] Systems were minimised using the steepest descent algorithm and subsequently equilibrated using a velocity-rescaling thermostat and Parrinello-Rahman barostat. All simulations were performed in explicit chloroform with three-dimensional periodic boundary conditions. See Supplementary Information for further details.

Scanning tunnelling microscopy (STM). Images were acquired with an Omicron STM-1 system operating under ultra-high vacuum (UHV) with a base pressure of 2×10^{-9} mbar. ***c*-P24b** was transferred from solution (toluene/methanol) to a clean Au(111) substrate using electrospray deposition[26,33]. Images were acquired at room temperature in constant current mode using electrochemically etched tungsten tips, coated in gold during tip optimisation.

All images taken at –1.8 V sample-bias, 20 pA set point current. See Supplementary Information for further details.

Optical spectroscopy. All measurements were carried out on solutions in toluene containing 1% pyridine (or neat toluene in the case of **T12** and ***c*-P24b·(T12)$_2$**), in silica cuvettes of size 3.5 × 10.0 mm or 10.0 × 10.0 mm, at a concentration of 0.25–2.0 μM for steady-state measurements and 0.25–2.0 mM for time-resolved experiments. Ultrafast time-resolved measurements were conducted using the photoluminescence upconversion (PL UC) technique. Samples were excited with a 410 nm pulse, generated by frequency doubling of a Ti:sapphire oscillator 820 nm output (Spectra Physics Mai-Tai, 100 fs, 80 MHz). The side-excitation configuration was adopted to avoid possible artefacts caused by self-absorption. In this configuration, the excitation beam entered the cuvette close to its front surface and PL was collected in the perpendicular direction with respect to the excitation beam by a pair of off-axis parabolic mirrors. The PL signal was then focused onto a beta-barium borate (BBO) crystal, mounted on a rotation stage to allow tuning of the phase-matching angle, and optically gated by a vertically polarised gate beam (820 nm) arriving at the BBO crystal at controllable time delays. The resulting PL UC signal generated by sum-frequency generation was then spectrally dispersed by a monochromator (Triax 190, Jobin-Yvon) and detected by a nitrogen-cooled CCD. A Schott filter UG11 was used to filter scattering from excitation and gate beams. The resulting time resolution was around 350 fs. Time-resolved spectra were corrected for instrument response by using a filament lamp of known emissivity. Time-integrated photoluminescence (TI PL) was measured by using the same spectrometer and CCD detector, while removing the BBO crystal and UG11 filter. Time-resolved PL dynamics at longer delay times (>1 ns) were measured by using the time-correlated single-photon counting technique with a temporal resolution of around 40 ps.

Data availability

All relevant data, including raw computational data etc as well as XYZ coordinates of calculated molecular geometries, are available within the paper and its Supplementary Information files, or have been deposited onto the Oxford Research Archive [34]. The NMR and STM data are presented in detail in the main Supplementary Information file and are available upon reasonable request from the authors.

Methods-only references

32. Abraham, M. J., Murtola, T., Schulz, R., Páll, S., Smith, J. C., Hess, B. & Lindahl, E. GROMACS: High performance molecular simulations through multi-level parallelism from laptops to supercomputers. *SoftwareX* **1–2**, 19–25, (2015).

33. Judd, C. J.; Kondratuk, D. V.; Anderson, H. L. & Saywell, A. On-surface synthesis within a porphyrin nanoring template. *Sci. Rep*. **9**, 9352 (2019).

34. Gotfredsen, H., Anderson, H. L., Deng, J., Van Raden, J., Righetto, M., Hergenhahn, J., Herz, L. M., Claridge, T. D. W., Duarte, F., Saywell, A., Clarke, M., Bellamy-Carter, A., Hart, J. & O'Shea, J. Dataset: Bending a photonic wire into ring. University of Oxford https://doi.org/10.5287/bodleian:44O2d5vKx (2022)